Wind velocity observation with a CW Doppler radar

Matti Lassas* Mustapha Mataich† Samuli Siltanen‡
Erkki Somersalo†

May 8, 2002

Abstract We study the problem of gathering information about wind velocity from continuous wave (CW) clear air Doppler radar measurements. The radar is assumed to be a monostatic fixed frequency Doppler radar and the wind velocity as well as the reflectivty are modeled as random fields with statistical parameters depending on the altitude. We seek to reconstruct the hodograph curve of the wind profile, i.e., the projection of the wind velocity profile to the ground plane. We show that under certain assumptions of the wind field, the problem reduces to a well known problem occurring in classical X-ray tomography. Numerical simulations based on the use of X-ray inversion methods are presented.

1 Introduction

The Doppler radar is a widely used instrument in meteorological applications and the literature on this topic is vast. In this work we are interested in clear air Doppler radar used for wind profiling. The main references for our discussion are e.g. [3, 4, 6]. It is well understood that, forgetting possible ambiguities, the ranging resolution of the Doppler radar is roughly inversely proportional to the bandwith of the radar (see e.g. [1, 8, 9]). On the other hand, due to the regulations concerning the use of rf ranging devices, it would be desirable to develop methods where the bandwidth is as narrow as possible, the device ultimately operating on a single frequency. Of, course, one cannot hope to get very detailed information of the weather conditions by using a fixed frequency device. It is our aim in this work to analyze how much information the fixed

*Rolf Nevanlinna Institute P.O. Box 4 (Yliopistonkatu 5) FIN-00014 University of Helsinki, Finland
†Institute of Mathematics Box 1100 FIN-02015 Helsinki University of Technology, Finland
‡Instrumentarium Corp. Imaging Division, Nahkelantie 160, P.O Box 20, FIN-04301 Tuusula, Finland

frequency signal carries and to develop computational methods to extract this information.

The paper is structured as follows: In Section 2, we derive a model for a single frequency CW radar signal scattered from a continuous moving random target. In particular, by using appropriate simplifying assumptions of the random structure of the target, we derive a formula the backscattered power spectrum. In Section 3, we apply this scattering model to derive a tomography formula for the recovery of of the hodograph curve of the wind profile. The inversion formula turns out to be a version of the inverse Radon transform. In section 4, the use of the reconstruction algorithm is demonstrated. In particular, we show that the hodograph curve contains information about the inflection points of the wind profile. Finally, in Section 5, a Monte Carlo simulation model is developed to demonstrate that the inversion formula can indeed be used even when the simplifying assumptions concerning the random structure of the target are not satisfied.

2 Scattering model

Clear air radars are based on the fact that even when no precipitation or overcast are present, the air contains enough micrometeors and turbulence to produce backscattering of rf waves, see e.g. [3, 6]. Since these scatterers move along with the wind, the Doppler effect gives information of the wind conditions.

In this section we derive the formulas describing the radar backscattering from the turbulent atmosphere. The general references in this section concerning the scattering of electromagnetic waves from a weak scatterer are [1, 3, 12]. The wind velocity as well as the atmospheric reflectivity are considered as random fields. In order to render the problem manageable, a number of simplifying assumptions of the random structure of the atmosphere are done. The assumptions are that

1. The velocity field and reflectivity are mutually independent random fields,
2. The correlation length of the random fields is negligible,
3. The velocity field is Gaussian.

In addition, in the next section where the hodograph curve is discussed and the tomography equation is derived, we further assume that

4. the atmospheric parameters depend on altitude only.

These assumptions are done here mostly for mathematical convenience. However, let us discuss them here briefly from the point of view of physics.

The assumption 1 is reasonable if we assume that most of the backscattering is due to micrometeors whose density is not correlated to the wind speed. On the other hand, large gradients in wind speed may cause more turbulence, suggesting that at least some correlation could exist. Such correlation is likely to be local, i.e., the wind speed and the relfectivity *at the same point* could be correlated. As we see later in the Monte Carlo simulations, this assumption can be abandoned but the forward model would become slightly more involved.

The assumption 2 means that individual scatterers are small and independent of each others. The simulations indicate that from the practical point of view this seems not to be a restrictive assumption.

One could use other probability distributions than the Gaussian ones in the discussion below as one can readily verify. However, the assumption 3 leads to a computationally nice closed form as the Gaussian probability density is completely determined by its first and second order statistics. Again, the simulation model shows that this restriction plays no crucial role in practice.

Finally, for the tomography algorithm, the assumption 4 is crucial since we are combining data from different look directions and our success to retrieve the hodograph curve depends on the reduction of the integral descibing the backscattered spectrum to a one dimensional integral with respect to the altitude only.

Consider the problem of recovering information of a turbulent wind velocity by using continuous wave monostatic Doppler radar operating at fixed angular frequency. We model the wind velocity $\mathbf{v}$ by a vector-valued field, written in Cartesian coordinates

$$\mathbf{v} = \mathbf{v}(\mathbf{r}) = (v_1(\mathbf{r}), v_2(\mathbf{r}), v_3(\mathbf{r})) \tag{1}$$

where $\mathbf{r}$ belongs to a layer $D = \{\mathbf{r} = (x, y, z) \in \mathbb{R}^3 : \ 0 < z < H\}$ modelling the atmosphere, the plane $r_3 = 0$ corresponding to the ground level.

Assume that the monostatic radar is at the origin $\mathbf{r} = 0$, sending a monochromatic time-harmonic signal $s_0(t) = e^{-i\omega_0 t}$ with angular frequency ω_0. The signal scatters back from the turbulence and impurities of the atmosphere that is modeled as a weakly scattering random structure. Assume that the scattering takes place in the far field region where the wave is approximated by a spherical wave. The received echo signal, after having mixed it down from ω_0 to zero, is approximated as

$$e(t) = \int_D \frac{\exp(-2ik\mathbf{v}\cdot\widehat{\mathbf{r}}t)}{r^2} g(\widehat{\mathbf{r}}, \widehat{\mathbf{r}}_0)\lambda(\mathbf{r})d\mathbf{r}, \quad \widehat{\mathbf{r}} = \frac{\mathbf{r}}{r}, \ r = |\mathbf{r}| \neq 0. \tag{2}$$

Here, $k = \omega_0/c$ is the wave number, $\lambda(\mathbf{r})$ is a complex reflectivity parameter at point $\mathbf{r}$ and $g(\widehat{\mathbf{r}}, \widehat{\mathbf{r}}_0)$ is the antenna directivity, $\widehat{\mathbf{r}}_0$ denoting the optical axis of the antenna. Possible atmospheric attenuation of the signal is included in our model to the reflectivity λ. To transform the signal into the frequency domain, let $W(t)$

denote a windowing function of a short integration interval $-T/2 \leq t \leq T/2$. Assuming that the atmospheric parameters do not alter significantly during this period, the windowed Fourier transform of the echo signal gives

$$e(\omega) = \int_{-T/2}^{T/2} e^{i\omega t} W(t) e(t) dt = \int_D \frac{g(\widehat{\mathbf{r}}, \widehat{\mathbf{r}}_0)}{r^2} \lambda(\mathbf{r}) \delta_T(\omega - 2k\widehat{\mathbf{r}} \cdot \mathbf{v}) d\mathbf{r}, \tag{3}$$

where

$$\delta_T(\omega) = \int_{-T/2}^{T/2} W(t) e^{i\omega t} dt \tag{4}$$

is an approximation of the Dirac delta. We repeat this measurement N times. During each interval of length T, the wind parameters are taken as constants with respect to time but they may change from sample to sample. By denoting the parameter values during the n:th integration as $\mathbf{v}_n$ and λ_n, we get a sample of the windowed Doppler spectra,

$$e_n(\omega) = \int_D \frac{g(\widehat{\mathbf{r}}, \widehat{\mathbf{r}}_0)}{r^2} \lambda_n(\mathbf{r}) \delta_T(\omega - 2k\widehat{\mathbf{r}} \cdot \mathbf{v}_n) d\mathbf{r}, \quad 1 \leq n \leq N. \tag{5}$$

We consider the atmospheric parameters as random fields. Consequently, the windowed spectra are also realizations of a random process $e(\omega)$ and the average power spectrum of this process is calculated as a sample average

$$P(\omega) = \mathrm{E}|e(\omega)|^2 \approx \frac{1}{N} \sum_{n=1}^{N} |e_n(\omega)|^2. \tag{6}$$

By substituting the expression (3), we obtain

$$P(\omega) = \int_D \int_D \frac{g(\widehat{\mathbf{r}}, \widehat{\mathbf{r}}_0) g(\widehat{\mathbf{r}'}, \widehat{\mathbf{r}}_0)}{r^2 r'^2} \mathrm{E}\left(\lambda(\mathbf{r}) \overline{\lambda(\mathbf{r}')} \delta_T(\omega - 2k\widehat{\mathbf{r}} \cdot \mathbf{v}) \overline{\delta_T(\omega - 2k\widehat{\mathbf{r}'} \cdot \mathbf{v}')} \right) d\mathbf{r} d\mathbf{r}', \tag{7}$$

where $\mathbf{v} = \mathbf{v}(\mathbf{r})$, $\mathbf{v}' = \mathbf{v}(\mathbf{r}')$. To simplify this expression, we assume that the reflectivity λ and the velocity field $\mathbf{v}$ are independent. By denoting the correlation function of the reflectivity as

$$C_\lambda(\mathbf{r}, \mathbf{r}') = \mathrm{E}(\lambda(\mathbf{r}) \overline{\lambda(\mathbf{r}')}), \tag{8}$$

we obtain

$$P(\omega) = \int_D \int_D \frac{g(\widehat{\mathbf{r}}, \widehat{\mathbf{r}}_0) g(\widehat{\mathbf{r}'}, \widehat{\mathbf{r}}_0)}{r^2 r'^2} C_\lambda(\mathbf{r}, \mathbf{r}') \mathrm{E}\left(\delta_T(\omega - 2k\widehat{\mathbf{r}} \cdot \mathbf{v}) \overline{\delta_T(\omega - 2k\widehat{\mathbf{r}'} \cdot \mathbf{v}')} \right) d\mathbf{r} d\mathbf{r}'. \tag{9}$$

To treat the velocity term, let us use the shorthand notation $v = \widehat{\mathbf{r}} \cdot \mathbf{v}(\mathbf{r})$, $v' = \widehat{\mathbf{r}}' \cdot \mathbf{v}(\mathbf{r}')$. Assume that v and v' have a joint probability distribution expressed by a probability density $p(v, v')$, i.e.,

$$P(v \in B, v' \in B') = \int_B \int_{B'} p(v, v') \, dv dv', \quad B, B' \subset \mathbb{R}. \tag{10}$$

Observe that the function p depends actually on $\mathbf{r}$ and $\mathbf{r}'$. With these notations, we get

$$P(\omega) = \int\int \frac{g(\widehat{\mathbf{r}}, \widehat{\mathbf{r}}_0) g(\widehat{\mathbf{r}'}, \widehat{\mathbf{r}}_0)}{r^2 r'^2} C_\lambda(\mathbf{r}, \mathbf{r}') D_v(\omega, \mathbf{r}, \mathbf{r}') d\mathbf{r} d\mathbf{r}', \tag{11}$$

where

$$D_v(\omega, \mathbf{r}, \mathbf{r}') = \int_{\mathbb{R}}\int_{\mathbb{R}} \delta_T(\omega - 2kv)\overline{\delta_T(\omega - 2kv')} p(v, v')\, dv dv'. \tag{12}$$

To simplify this expression even further, assume that $\mathbf{v}(\mathbf{r})$, and thus v, is a Gaussian field. Let the mean and covariance be

$$\mathrm{E}v(\mathbf{r}) = v_0(\mathbf{r}), \quad \mathrm{E}((v(\mathbf{r}) - v_0(\mathbf{r}))(v(\mathbf{r}') - v_0(\mathbf{r}'))) = C_v(\mathbf{r}, \mathbf{r}'). \tag{13}$$

Further, by writing

$$\Sigma = \Sigma(\mathbf{r}, \mathbf{r}') = \begin{pmatrix} C_v(\mathbf{r}, \mathbf{r}) & C_v(\mathbf{r}, \mathbf{r}') \\ C_v(\mathbf{r}', \mathbf{r}) & C_v(\mathbf{r}', \mathbf{r}') \end{pmatrix} \tag{14}$$

and $v_0 = v_0(\mathbf{r})$, $v_0' = v_0(\mathbf{r}')$, respectively, the joint probability distribution of v and v' is given by

$$p(v, v') = \frac{1}{2\pi\sqrt{\det \Sigma}} \exp\left(-\frac{1}{2}(v - v_0, v' - v_0')\Sigma^{-1} \begin{pmatrix} v - v_0 \\ v' - v_0' \end{pmatrix} \right). \tag{15}$$

If we assume that δ_T is a good approximation for the Dirac delta function (i.e., the integration interval T is sufficiently long), we have

$$\begin{aligned} D_v(\omega, \mathbf{r}, \mathbf{r}') &\approx \int_{\mathbb{R}}\int_{\mathbb{R}} \delta(\omega - 2kv)\delta(\omega - 2kv') p(v, v') dv dv' \\ &= \frac{1}{4k^2} p\left(\frac{\omega}{2k}, \frac{\omega}{2k}\right). \end{aligned} \tag{16}$$

Observe that the function $\omega \mapsto D_v(\omega, \mathbf{r}, \mathbf{r}')$ is in fact a Gaussian function. In particular, if we assume that $C_v(\mathbf{r}, \mathbf{r}') = 0$ if $\mathbf{r} \neq \mathbf{r}'$, i.e., the correlation length is negligible, and denote $C_v(\mathbf{r}, \mathbf{r}) = C_v(\mathbf{r})$, we have

$$\begin{aligned} D_v(\omega, \mathbf{r}, \mathbf{r}') &= \frac{1}{8\pi k^2 \sqrt{C_v(\mathbf{r}) C_v(\mathbf{r}')}} \exp\Bigg(-\frac{1}{8k^2}\Bigg(\frac{1}{C_v(\mathbf{r})}(\omega - 2kv_0)^2 \\ &\qquad + \frac{1}{C_v(\mathbf{r}')}(\omega - 2kv_0')^2 \Bigg)\Bigg). \end{aligned} \tag{17}$$

As a further simplification, we consider the case when also the correlation length of λ is zero. This is expressed by

$$C_\lambda(\mathbf{r}, \mathbf{r}') = C_\lambda(\mathbf{r})\delta_3(\mathbf{r} - \mathbf{r}'). \tag{18}$$

With this approximation, the formula for the power spectrum reduces to

$$\begin{aligned} P(\omega) &= \int_D \frac{g(\widehat{\mathbf{r}},\widehat{\mathbf{r}}_0)^2}{r^4} C_\lambda(\mathbf{r}) D_v(\omega,\mathbf{r},\mathbf{r}) d\mathbf{r} \qquad (19) \\ &= \frac{1}{8\pi k^2}\int_D \frac{g(\widehat{\mathbf{r}},\widehat{\mathbf{r}}_0)^2}{r^4}\frac{C_\lambda(\mathbf{r})}{C_v(\mathbf{r})} \exp\left(-\frac{1}{4k^2 C_v(\mathbf{r})}(\omega - 2kv_0)^2\right) d\mathbf{r} \end{aligned}$$

This formula will be used as a starting point in subsequent modelling.

3 Hodograph curve

In the previous section, we derived an approximate formula (19) for the power spectrum, and the task is to estimate the average wind velocity as well as the autocorrelations of the velocity and reflectivity. The only free parameter at our disposal in formula (19) is the look direction $\widehat{\mathbf{r}}_0$ of the radar. It is clear that without simplifying assumptions, the task is hopeless. However, it turns out that in some cases, useful information can be extracted from this data. Let us mention that the discussion here has a resemblance with so called vector tomography, see [2, 10, 11].

To begin, we fix some notations. Let β denote the elevation angle of the radar, $\beta = \pi/2$ corresponding to the zenith. By θ we denote the azimuth angle of the radar, $\theta = 0$ being the positive x–axis. With these notations,

$$\widehat{\mathbf{r}}_0 = \cos\beta\cos\theta\widehat{\mathbf{e}}_1 + \cos\beta\sin\theta\widehat{\mathbf{e}}_2 + \sin\beta\widehat{\mathbf{e}}_3. \qquad (20)$$

For later use, we write out the dependence of the power spectrum of the radar look angles as $P(\omega) = P(\omega,\beta,\theta)$.

In this section, we make the simplifying assumption that the atmospheric parameters depend on the altitude z only, and write

$$C_\lambda(\mathbf{r}) = c_\lambda(z), \quad C_v(\mathbf{r}) = c_v(z), \quad \mathbf{v}_0 = \mathbf{v}_0(z). \qquad (21)$$

For further simplifications, assume that the radar has a narrow beam form so that we can make the approximation

$$\widehat{\mathbf{r}}\cdot\mathbf{v}_0(z) \approx \widehat{\mathbf{r}}_0\cdot\mathbf{v}_0(z) \qquad (22)$$

in the cone where $g(\widehat{\mathbf{r}},\widehat{\mathbf{r}}_0)$ is not negligible. On the other hand, by a geometric argument, we see that denoting by T_z the plane parallel to Earth's surface at the altitude $z > 0$, we have

$$\int_{T_z} \frac{g(\widehat{\mathbf{r}},\widehat{\mathbf{r}}_0)^2}{r^4} dA = \frac{K(\beta)}{z^2}, \qquad (23)$$

where $K(\beta)$ is a geometric constant depending on the elevation angle and the beam form of the radar. With these approximations, the formula of the power spectrum (19) assumes the form

$$P(\omega,\beta,\theta)=\frac{K(\beta)}{8\pi k^2}\int_0^\infty \frac{1}{z^2}\frac{c_\lambda(z)}{c_v(z)}\exp\left(-\frac{1}{4k^2c_v(z)}(\omega-2k\widehat{\mathbf{r}}_0\cdot\mathbf{v}_0(z))^2\right)dz. \quad (24)$$

By denoting the altitude-dependent variance as

$$\sigma(z)^2=2k^2c_v(z) \quad (25)$$

and defining a density function $\Phi(z)$ as

$$\Phi(z,\beta)=\frac{K(\beta)}{4\sqrt{2\pi}k^2}\frac{c_\lambda(z)}{z^2\sqrt{c_v(z)}}, \quad (26)$$

the formula (24) reads as

$$P(\omega,\beta,\theta)=\int_0^\infty \Phi(z,\beta)G_{\sigma(z)}(\omega-2k\widehat{\mathbf{r}}_0\cdot\mathbf{v}_0(z))dz, \quad (27)$$

where $G_{\sigma(z)}$ is a Gaussian function with variance $\sigma(z)^2$,

$$G_{\sigma(z)}(t)=\frac{1}{\sqrt{2\pi}\sigma(z)}\exp\left(-\frac{1}{2\sigma(z)^2}t^2\right). \quad (28)$$

Assume now that the average wind velocity $\mathbf{v}_0$ is parallel to the Earth's surface, i.e.,

$$\mathbf{v}_0(z)=v_0(z)(\widehat{\mathbf{e}}_1\cos\alpha(z)+\widehat{\mathbf{e}}_2\sin\alpha(z)). \quad (29)$$

Here, $v_0(z)$ is the average speed profile and $\alpha(z)$ is the average wind direction angle. Following [4], we define the *hodograph curve* corresponding to the average wind velocity as a planar curve

$$z\mapsto(v_0(z)\cos\alpha(z),v_0(z)\sin\alpha(z)) \quad (30)$$

parametrized by the altitude. The knowledge of the hodograph curve (without its parameterization) would give us the dependence of the speed profile to the wind direction,

$$v_0=v_0(\alpha). \quad (31)$$

Observe that this function can be multi-valued. This knowledge is insufficient, in general, to determine the velocity profile as a function of altitude, since it carries no information of the parameterization with respect to the altitude.

To clarify the concept of a hodograph curve, consider Figure 1, where the spatial curve depicts the the average velocity vector, i.e., the function

$$z\mapsto(v_{0x}(z),v_{0y},z), \quad (32)$$

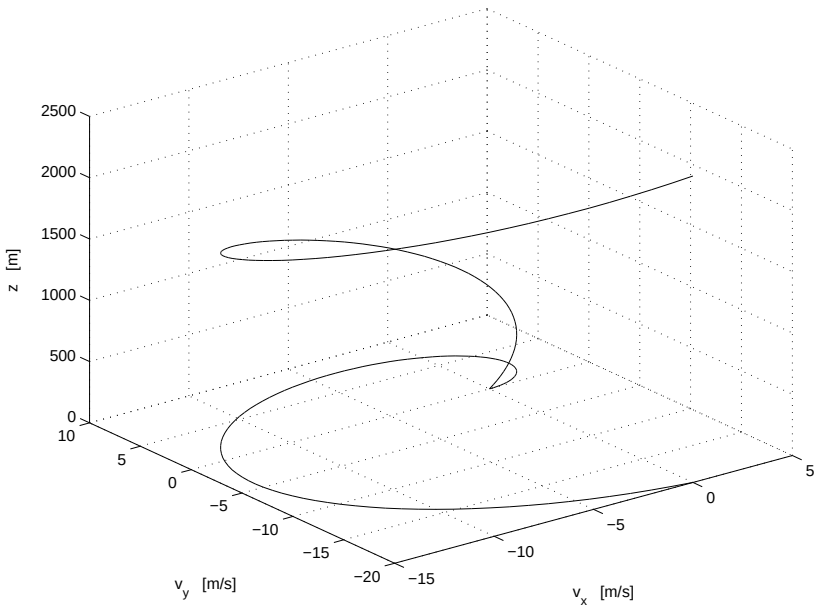

Figure 1: An average wind profile and its projection to the xy-plane, the hodograph curve.

while the projection to the plane $z = 0$ is the corresponding hodograph curve.

The problem considered here is, how to reconstruct the hodograph curve by monochromatic Doppler radar measurements. We show here that the above model allows us to write the radar echo approximately as a Radon transform of the hodograph density. Consequently, the hodograph density can be recovered by standard tomographic methods.

Consider the following measurement. The elevation angle $\beta > 0$ is kept fixed, and the azimuth angle θ is varied from $\theta = 0$ to $\theta = \pi$. from this data, the goal is to estimate the hodograph curve. Let us denote

$$\widehat{\mathbf{s}}(\theta) = \cos\theta\,\widehat{\mathbf{e}}_1 + \sin\theta\,\widehat{\mathbf{e}}_2, \tag{33}$$

and

$$\mathbf{p}(z) = 2k\cos\beta v_0(z)(\cos\alpha(z)\widehat{\mathbf{e}}_1 + \sin\alpha(z)\widehat{\mathbf{e}}_2). \tag{34}$$

By suppressing the dependence of the fixed elevation angle, the power spectrum reads

$$P(\omega,\theta) = \int_0^\infty \Phi(z) G_{\sigma(z)}(\omega - \widehat{\mathbf{s}}(\theta)\cdot\mathbf{p}(z))dz. \tag{35}$$

We rewrite this integral in a slightly different form. Let us denote by δ_2 the Dirac delta function in $\mathbb{R}^2$. Then, we obtain

$$P(\omega,\theta) = \int_0^\infty \Phi(z) \int_{\mathbb{R}^2} \delta_2(\mathbf{q} - \mathbf{p}(z)) G_{\sigma(z)}(\omega - \widehat{\mathbf{s}}(\theta)\cdot\mathbf{q})d\mathbf{q}dz. \tag{36}$$

Consider first this function when the variance of the Gaussian G_σ goes to zero, i.e., $\sigma \to 0$. The Gaussian function tends to the Dirac delta and $P(\omega,\theta) \to P_0(\omega,\theta)$, where

$$P_0(\omega,\theta) = \int_0^\infty \Phi(z) \int_{\mathbb{R}^2} \delta_2(\mathbf{q}-\mathbf{p}(z))\delta(\omega - \widehat{\mathbf{s}}(\theta)\cdot\mathbf{q})d\mathbf{q}dz. \tag{37}$$

This function can be written as

$$P_0(\omega,\theta) = \int_{L(\omega,\theta)} \gamma(\mathbf{q})d\ell(\mathbf{q}), \tag{38}$$

where $L(\omega,\theta)$ is the line

$$L(\omega,\theta) = \{\mathbf{q}\in\mathbb{R}^2 \mid \widehat{\mathbf{s}}(\theta)\cdot\mathbf{q} = \omega\}, \tag{39}$$

and the density γ is given by the formula

$$\gamma(\mathbf{q}) = \int_0^\infty \Phi(z)\delta_2(\mathbf{q}-\mathbf{p}(z))dz. \tag{40}$$

In other words, the ideal power spectrum $P_0(\omega,\theta)$ is a Radon transform (or X-ray transform) of a density $\gamma(\mathbf{q})$, and this density is non–zero only if $\mathbf{q}$ lies on the hodograph curve. As a technical detail, we note that the density γ is given as

$$\gamma(\mathbf{q}) = \sum_{j=1}^n \frac{\Phi(z_j)}{\beta_j}, \tag{41}$$

where the point z_j are the points of intersection of the curve $\mathbf{p}(z)$ and the line $L(\omega,\theta)$ (assumed to be finitely many) and

$$\beta_j = \frac{d}{dz}(\widehat{\mathbf{s}}(\theta)\cdot\mathbf{p}(z))\big|_{z=z_j}, \quad 1\le j\le n. \tag{42}$$

Evidently, the density γ has singularities at inversion points where the derivative of $\mathbf{p}(z)$ with respect to z vanishes.

It would be tempting to say that the limit $\sigma \to 0$ corresponds to the case when the wind speed has zero variance, i.e., $c_v \to 0$. However, the situation is slightly more complicated since the density function Φ depends on the variance c_v through formula (26).

Let us denote the Radon transform as

$$(\mathcal{R}f)(\omega,\theta) = \int_{L(\omega,\theta)} f(\mathbf{q})d\ell(\mathbf{q}). \tag{43}$$

The Radon transform is fundamental object studied in X-ray tomography (see e.g. [5, 7]) and it has an inverse transform given by formula

$$(\mathcal{R}^{-1}F)(\mathbf{q}) = -\frac{1}{2\pi^2}\int_0^{2\pi}\int_0^\infty \frac{\partial F}{\partial\omega}(\omega+\mathbf{q}\cdot\widehat{\mathbf{s}}(\theta),\theta)\,\frac{d\omega}{\omega}d\theta, \quad \mathbf{q}\in\mathbb{R}^2. \tag{44}$$

Thus in the case where $\sigma(\mathbf{r}) = 0$, the hodograph curve can be recovered by applying the inverse transform on the power spectrum P_0 to get

$$\gamma(\mathbf{q}) = (\mathcal{R}^{-1}P_0)(\mathbf{q}). \tag{45}$$

Based on this formula, it is natural to apply the inverse Radon transform on the power spectrum also in the case $\sigma \neq 0$ and hope that some useful information of the hodograph curve is obtained. Let us define

$$h(\mathbf{q}) = (\mathcal{R}^{-1}P)(\mathbf{q}). \tag{46}$$

The question that we study is, how the function h is related to the density γ and ultimately to the hodograph curve. Assume that the variance σ is a non-zero but constant with respect to the altitude. In this case, we observe that

$$P(\omega, \theta) = G_\sigma * P_0(\omega, \theta), \tag{47}$$

where the convolution $*$ is understood with respect to the frequency ω. To study the density h in this case, we remind the reader of the well known connection between the inverse Radon transform formula and Fourier analysis. By applying the one-dimensional Fourier transform $\mathcal{F}_1$ with respect to ω on P, we obtain

$$\mathcal{F}_1 P(t, \theta) = \int_{-\infty}^{\infty} e^{-i\omega t} P(\omega, \theta) d\omega = \widehat{G}_\sigma(t) \mathcal{F}_1 P_0(t, \theta) \tag{48}$$

by the convolution theorem, where $\widehat{G}_\sigma$ is the Fourier transform of G_σ,

$$\widehat{G}_\sigma(t) = \int_{-\infty}^{\infty} e^{-i\omega t} G_\sigma(\omega) d\omega = e^{-\frac{1}{2}\sigma^2 t^2}. \tag{49}$$

On the other hand, by formula

$$\mathcal{R}f(\omega, \theta) = \int_{\mathbb{R}^2} f(\mathbf{q}) \delta(\omega - \mathbf{q} \cdot \widehat{\mathbf{s}}(\theta)) d\mathbf{q} \tag{50}$$

it is evident that

$$\mathcal{F}_1 \mathcal{R} f(t, \theta) = \int_{\mathbb{R}^2} e^{-it\widehat{s}\cdot\mathbf{q}} f(\mathbf{q}) d\mathbf{q} = \mathcal{F}_2 f(t\widehat{\mathbf{s}}), \tag{51}$$

so the inverse radon transform can be written as

$$\mathcal{R}^{-1}F(\mathbf{q}) = \mathcal{F}_2^{-1}\mathcal{F}_1 f(\mathbf{q}), \tag{52}$$

where it is understood that the inverse transform of the two-dimensional Fourier transform $\mathcal{F}_2$ is calculated by integrating with respect to the variable $\mathbf{t} = t\widehat{\mathbf{s}}$ over $\mathbb{R}^2$. By this formula and the convolution theorem in $\mathbb{R}^2$, we find that

$$h(\mathbf{q}) = H_\sigma * \gamma(\mathbf{q}), \tag{53}$$

where the convolution is understood over $\mathbb{R}^2$ and the function H_σ is obtained as

$$H_\sigma(\mathbf{q}) = \mathcal{F}_2^{-1}[\hat{G}_\sigma(|\ \cdot\ |)](\mathbf{q}). \tag{54}$$

Explicitly, we have

$$H_\sigma(\mathbf{q}) = \left(\frac{1}{2\pi}\right)^2 \int e^{i\mathbf{t}\cdot\mathbf{q}} e^{-\frac{1}{2}\sigma^2|\mathbf{t}|^2} d\mathbf{t} = \frac{1}{2\pi\sigma^2} e^{-\frac{1}{2\sigma^2}|\mathbf{q}|^2}. \tag{55}$$

This means that in the case of constant variance, an application of the inverse Radon transform gives a density that is not strictly supported on the hodograph curve but rather a blurred density, the blurring function being a radial Gaussian function whose width is proportional to the standard deviation of the velocity profile above the hodograph curve.

To deal with the more general case when $\sigma \neq$ constant, we make the piecewise constant approximation. Let us divide the atmosphere in layers at altitudes $0 = z_0 < z_1 < \ldots < z_K$, where z_K is the maximum altitude of practical interest, and assume that

$$\sigma(z) \approx \sigma_j \text{ for } z_{j-1} < z \leq z_j,\ 1 \leq j \leq K. \tag{56}$$

Then, the power spectrum (36) reads as

$$\begin{aligned} P(\omega,\theta) &= \sum_{j=1}^{K} \int_{z_{j-1}}^{z_j} \Phi(z) \int_{\mathbb{R}^2} \delta_2(\mathbf{q} - \mathbf{p}(z)) G_{\sigma_j}(\omega - \widehat{\mathbf{s}}(\theta)\cdot\mathbf{q}) d\mathbf{q} dz \\ &= \sum_{j=1}^{K} G_{\sigma_j} * P_{0j}(\omega,\theta), \end{aligned} \tag{57}$$

where

$$P_{0j} = \int_{z_{j-1}}^{z_j} \Phi(z)\delta_2(\mathbf{q} - \mathbf{p}(z))\delta(\omega - \hat{\mathbf{s}}\cdot\mathbf{q}) d\mathbf{q} dz, \tag{58}$$

and the convolution is with respect to the Doppler frequency ω. The same argument as before gives now that by applying the inverse Radon transform on P, we obtain

$$h(\mathbf{q}) = (\mathcal{R}^{-1}P)(\mathbf{q}) = \sum_{j=1}^{K} H_{\sigma_j} * \gamma_j(\mathbf{q}), \tag{59}$$

where

$$\gamma_j(\mathbf{q}) = \int_{z_{j-1}}^{z_j} \Phi(z)\delta_2(\mathbf{q} - \mathbf{p}(z)) dz, \tag{60}$$

i.e., the portion of the hodograph curve that corresponds to the wind profile in the j:th layer. This means that the reconstructed function h is again a blurred image of the true hodograph curve with a variable blurring function.

4 Numerical results

In this section, we demonstrate with numerical simulations the reconstruction method discussed in the previous sections. In this preliminary study, artificially produced data is used as real data is not available to us.

The discussion is divided in two parts. In the first one, the data simulation is based on the forward model for the power spectrum derived in Section 3. Since the inversion method is based on the same formula, the results are overly optimistic and should be understood as a demonstration of the method in the most favorable conditions when all the assumptions of Section 2 concerning the velocity fields are valid. In the second part, the data is generated using a Monte Carlo simulation model. Here, we demonstrate that the inversion scheme produces reasonable results even when the rather strong assumptions are violated.

4.1 Simulation with the forward model

In our examples presented in this part of the study, the simulated data is based on the formula

$$P(\omega,\theta) = \int_0^\infty \Phi(z) G_\sigma(\omega - \hat{\mathbf{s}}(\theta)\cdot\mathbf{p}(z))dz, \tag{61}$$

where the deviation σ of the Gaussian G_σ is kept constant. In all our simulations, the elevation angle is $\beta = 60°$. The integration over the altitude z is performed from an effective minimum value corresponding to the beginning to the wave field, denoted by h, up to an effective maximum radar range H. In our simulation, we have chosen $h = 200$m, $H = 2500$m. These figures are reasonable ones for a radar functioning at the central frequency $f_0 = 1$GHz, where $f_0 = \omega_0/2\pi$, although considerable variations may occur depending upon meteorological conditions [6].

The effective reflectivity contains the atmospheric attenuation effect. To model the attenuation, we use Beer's law, i.e., we assume that the attenuation factor is of the form

$$\Phi(z) \sim \exp\left(-2\int_0^z \mu_{\mathrm{a}}(z')dz'\right), \tag{62}$$

the function μ_{a} being the effective absorption coefficient accounting fo absoption and scattering. In our simulation, we use $\mu_{\mathrm{a}} =$ constant. To make the model more realistic, the function values $\Phi(z_j)$ at the points of integration are multiplied by a random component drawn from uniform distribution, $\Phi(z_j) \sim u$, $u \sim \mathcal{U}([0,1])$. This randomness reflect our uncertainty of the reflectivity upon the atmospheric conditions.

In the first example, the wind profile is assumed to form a spiral on the hodograph plane, see Figure 1. Here, the wind speed is assumed to increase linearly

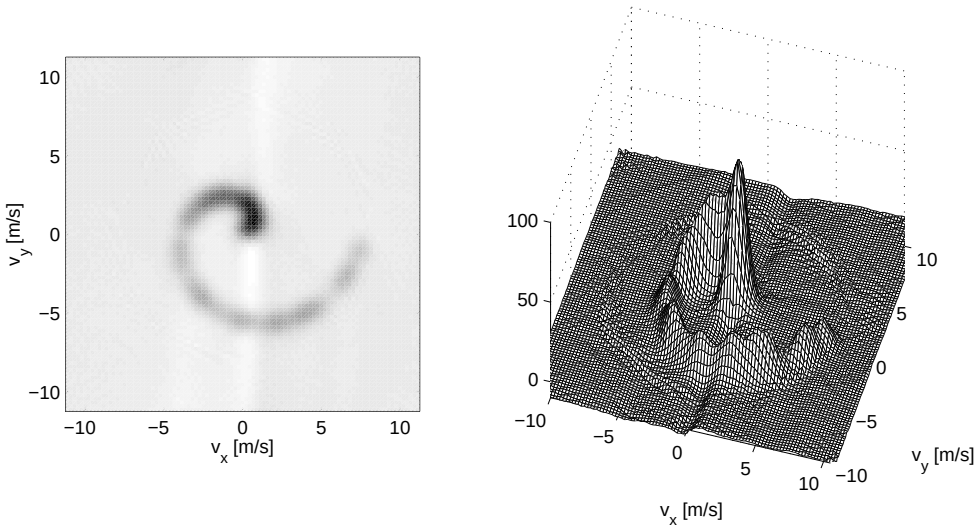

Figure 2: A tomographic reconstruction of the hodograph curve corresponding to the wind profile of Figure 1.

from zero to the maximum value 7.5 m/s such that the mean velocity vector is parallel to the ground surface and turning a full circle. In this simulation, the attenuation was ignored, i.e., $\mu_{\mathrm{a}} = 0$. The deviation parameter σ was constant in this example, having the value $\sigma = 10\ \mathrm{s}^{-1}$. Translated in terms of the velocity, this corresponds to about 0.5 m/s standard deviation in the wind speed parallel to the ground surface.

The Radon inversion was performed by using the standard Algebraic Reconstruction Technique, ART (see [5] for a detailed discussion of the method). We use the ART as a regularization scheme and perform only one full iteration round to control the noise in the reconstruction. Figure 2 represents the reconstruction as a projected density plot and a three dimensional surfece plot. The correct hodograph curve is plotted for comparison in the projected image. We see that, in accordance to the previous discussion, the reconstructed curve corresponds to a blurring of the original curve by a Gaussian kernel.

The second example demonstrates the effect of singular (or inflection) points of the wind profile, i.e., those values of the altitude parameter z when

$$\frac{d}{dz}\big(\hat{\mathbf{s}}(\theta)\cdot\mathbf{p}(z)\big) = 0, \quad \omega - \hat{\mathbf{s}}(\theta)\cdot\mathbf{p}(z) = 0. \tag{63}$$

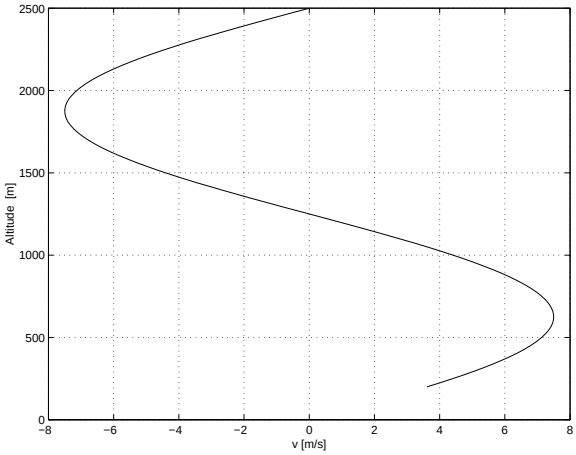

,

Figure 3: The wind velocity profile as a function of altitude, the direction being constant.

As formula (41) suggests, the hodograph curve becomes singular at these points, and consequently the blurred curve should have high values at those points. This fact contains implicit information of the altitude dependence of the profile and could therefore turn useful in practice.

In this example, the average wind speed is parallel to a line in xy–plane with values depicted in Figure 3.

In this example, the altitude attenuation is included such that $\mu_{\mathrm{a}} = -\log(0.75)/H$, i.e., the backscattered signal e has attenuated 75% of the initial value at maximum altitude. With otherwise the same parameter values as in the first example, we reconstruct the hodograph curve by using the ART algorithm. In Figure 3, the reconstruction is depicted. The effect of the singular points to the reconstructed hodograph curve are clearly seen as high peak values as predicted by the theory.

In the third example, we use a true wind profile as a starting point of the simulation. The wind velocity at different altitudes are measured by a weather balloon but the power spectrum is still a simulated one as before. Figure 4 depicts the corresponding hodograph curve as a solid line plotted on top of the ART based reconstruction. In this figure, the standard deviation was $\sigma = 10\,\mathrm{s}^{-1}$.

4.2 Monte Carlo simulation model

To test the inversion model and its robustness, we generate the data in this section using a Monte Carlo model based on an ensemble of single random

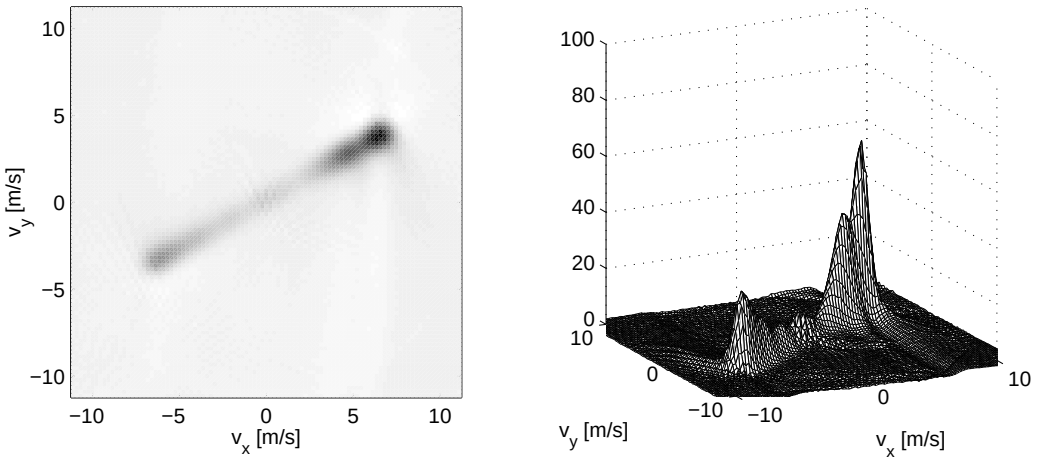

Figure 4: Tomographic resonstruction of the hodograph curve obtained from the profile in Figure 3.

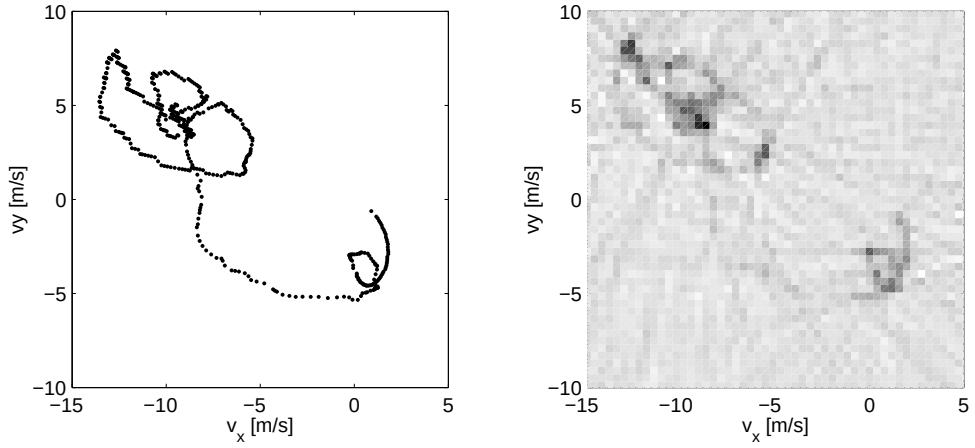

Figure 5: A true hodogrpah curve obtained from a weather balloon measurement and a reconstruction based on the forward model simulation.

scatterers. The starting point here is the formula for a single windowed Doppler spectrum (5). We assume that the echo e_n is due to small point scatterers at various altitudes in the interval $[h, H]$. Thus, the approximate formula for a single windowed Fourier spectrum becomes

$$e_n(\omega) \approx \sum_{j=1}^{M} \frac{g(\widehat{\mathbf{r}}_j, \widehat{\mathbf{r}}_0)}{r_j^2} \lambda(z_j) \delta_T(\omega - 2k\widehat{\mathbf{r}}_\mathbf{j} \cdot \mathbf{v}_j), \tag{64}$$

where M is the sample size. Having produced a sample $\{e_1(\omega), \ldots, e_N(\omega)\}$ of the simulated echoes for each azimuth angle θ, the power spectra are then computed as sample avarages according to formula (6). In formula (64), the scatterer locations $\mathbf{r}_j$ as well as the parameter values $\lambda(\mathbf{r}_j)$ and $\mathbf{v}_j$ are random quantities that are drawn from appropriate probability distributions as explained below.

First, we fix the average wind profile $(v_0(z), \alpha(z))$ as well as the wind speed and wind direction variances, $(\sigma_v(z)^2, \sigma_\alpha(z)^2)$.

The first step is to draw randomly the scatterer altitudes z_j, $1 \leq j \leq M$. The scatterers are assumed to have uniform distribution in a given altitude interval $[h, H]$. However, the radar beam widens out as $\sim z^2$ with respect to the altitude, so the radar sees more scatterers higher up. Therefore, the probability density is

$$\pi(z) \sim z^2, \quad h \leq z \leq H. \tag{65}$$

Precisely, the probability distribution function is

$$\Phi(z) = \int_h^z \pi(z')dz' = \frac{z^3 - h^3}{H^3 - h^3}, \quad h \leq z \leq H. \tag{66}$$

In practice, we draw independently random variables $t_j \sim \mathcal{U}([0, 1])$, the uniform distribution, and set

$$z_j = \Phi^{-1}(t_j) = H(a + (1 - a)t_j)^{1/3}, \quad a = \left(\frac{h}{H}\right)^3. \tag{67}$$

The next step is to produce the velocity vectors of the scatterers. To this end, we define the velocity vectors

$$\mathbf{v}_j = v_0(z_j)(\mathbf{e}_1 \cos\alpha(z_j) + \mathbf{e}_2 \sin\alpha(z_j)) + \delta\mathbf{v}_j, \tag{68}$$

where the random perturbation $\delta\mathbf{v}_j$ has normally distributed components,

$$\delta v_{j\nu} \sim \mathcal{N}(0, \sigma(z_j)^2), \quad \nu = x, y, z. \tag{69}$$

Observe that we allow the scatterers to have a non-zero vertical component, too. Having computed the velocities, we draw randomly the reflectivities. By using the Bayes formula for probability densities, i.e.,

$$\pi(\lambda, \mathbf{v}) \sim \pi(\lambda \mid \mathbf{v})\pi(\mathbf{v}), \tag{70}$$

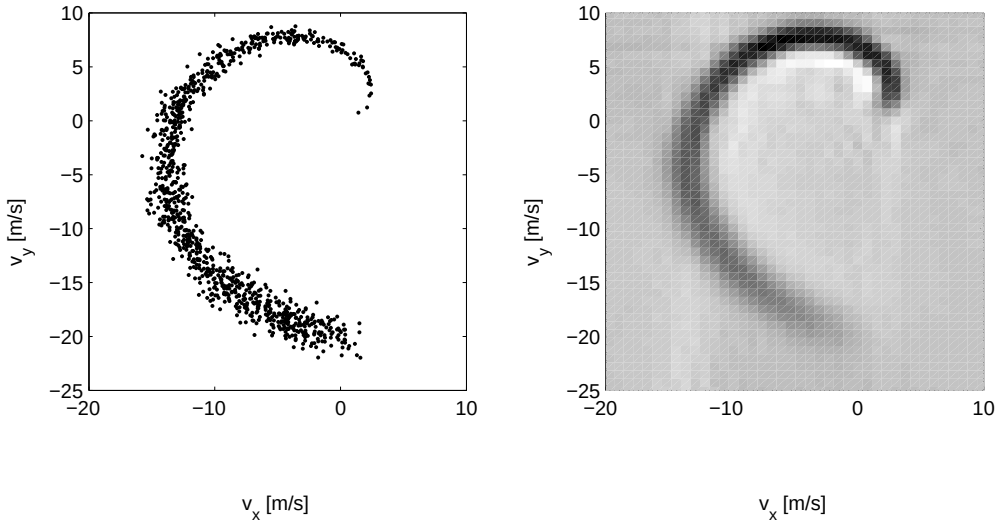

Figure 6: One sample of simulated velocities projected to the ground level (left) and the reconstructed hodograph curve computed from the Monte Carlo simulated data (right).

we can draw the quantities $\lambda_j = \lambda(z_j)$ either independently of $\mathbf{v}_j$ by setting $\pi(\lambda \mid \mathbf{v}) = \pi(\lambda)$ or by correlating them with the already drawn velocities. In the numerical tests, both options are tested.

Having these quantities computed, we can calculate the Fourier spectra of formula (64). We add to each e_n additive independent noise to account for effects that have not been modelled, such as relections from low-altitude perturbations, ground clutter, birds and insects etc.

In the first test, we use the same mean wind profile is the one shown in Figure 1. The number of single scatterers is $M = 1000$ and the number of independent spectra e_n per azimuth angle θ is $N = 50$. The wind speed standard deviation $\sigma(z)$ is 5% of the mean velocity $v_0(z)$, and the reflectivities λ_j are drawn independently of the velocities, following the law

$$\lambda_j \sim \text{Rayleigh}(\gamma_j), \quad \gamma_j = \exp(-\mu_a z_j). \tag{71}$$

Here, the absorption coefficient is chosen again as $\mu_a = 1/H$.

In our simulation, the windowing function W was simply taken as a box-car function with the time parameter chosen as $T = 0.15\,\text{s}$. With this choice, the distance of the first sidelobes of the sinc–function from the mean frequency is about $31\,\text{s}^{-1}$, which in terms of the Doppler shift correspond to $0.75\,\text{m/s}$ velocity in the radial direction. With these parameter values, the total measurement time per azimuth direction would be $NT = 10\,\text{s}$.

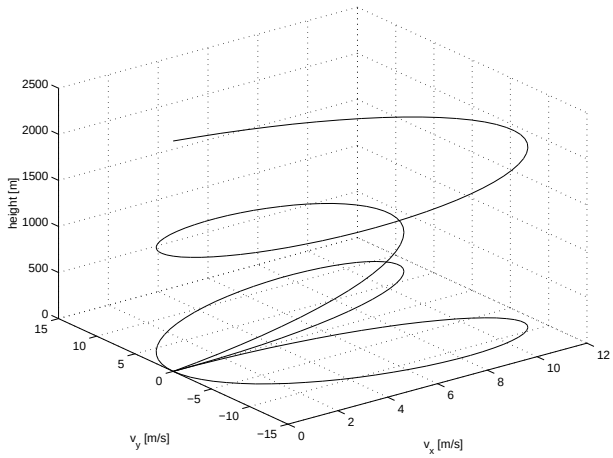

,

Figure 7: True wind profile and the corresponding hodograph curve.

In Figure 6, we have depicted the randomly drawn velocity values corresponding to a single simulated backscattered echo (left). In the same figure (right), the two dimensional projection of the reconstructed hodograph curve is shown.

As a final example, we consider the case where the wind speed and the reflectivities are not independent. In this example, the reflectivity $\lambda_j = \lambda(z_j)$ is drawn from the conditional density of the form

$$\lambda_j \sim \pi(\lambda \mid v_j) = \text{Rayleigh}(|\mathbf{v}_j|\gamma_j), \quad \gamma_j = \exp(-\mu_a z_j). \tag{72}$$

This is a model where it is assumed that the increased wind velocity causes increased turbulence and thus produces a stronger backscattering effect. The other parameters are as in the previous example. Finally, normally distributed random noise with standard deviation 3% of the maximum signal level was added to each simulated acho e_n signal before summing up to form the power spectrum.

The true wind profile is shown in Figure 7. Again, a sample of 1000 scatterer velocities as well as the reconstructed hodograph curve are displayed in Figure 8. Here we see that the added noise contributes mostly to an elevated background noise level in the reconstruction, while the hodograph information is still clearly visible.

5 Discussion

Starting from a simplified stochastic scattering model, we have derived an approximation for the monochromatic monostatic radar echo from the atmosphere

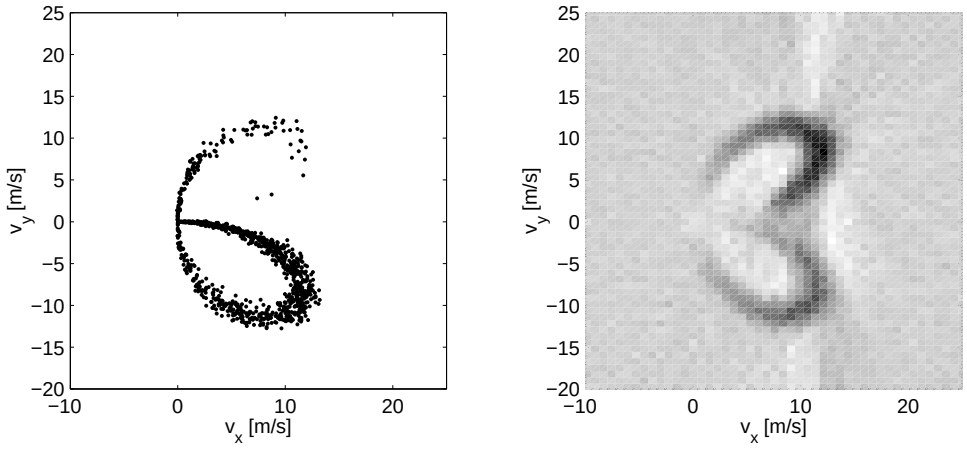

Figure 8: One sample of simulated velocities projected to the ground level (left) and the reconstructed hodograph curve computed from the Monte Carlo simulated data (right).

with variable windspeed. Keeping the elevation angle of the radar fixed and scanning in the azimuth direction, we showed that the power spectrum is a blurred Radon transform of the hodograph curve of the wind profile, i.e., the projection of the wind vector to the ground surface. Also, we showed that by applying the inverse Radon transform to this data we obtain a blurred image of the hodograph curve, the blurring depending of the stochastic variances in the wind speed and the reflectivity of the air layers. To test the feasibility of the method to estimate the hodograph curve, we applied the suggested algorithm to numerically simulated data. The Radon inversion was based on the standard ART algorithm. Currently, the authors have not access to real CW radar data.

In this article, the question of retrieving altitude information from the hodograph curve was left open. This information cannot be obtained reliably with a non-ranging single frequency CW instrument. Some information can be obtained by assuming attenuation models of the signal, but this sort of assumptions are highly unreliable and their practical value requires further analysis. Another idea of getting altitude information is to use several elevation angles combined with the azimuthal scanning and attenuation modelling. These ideas are not tested in this work.

References

[1] Blahut R E, Miller Jr. W, Wilcox C H (1991) Radar and Sonar, Part I. Springer-Velag New York.

[2] Denisov A M, Popov A A (1996) A two-dimensional Doppler tomography problem (Russian) Zh. Vychisl. Mat. i Mat. Fiz. 36 , no. 11, pp. 126-133. Translation in Comput. Math. Math. Phys. 36 (1996), no. 11, pp. 1591–1598.

[3] Doviak R J, Zrnic D S (1993) Doppler Radar and Weather Observations. Second Edition. Academic Press, Inc.

[4] Gorelik A G, Sterlyadkin V V (1990) Doppler Tomography in Radar Meteorology. Izvestiya, Atmospheric and Oceanic Physics 26, pp. 28–33.

[5] Natterer F (1986) The Mathematics of Computerized Tomography. John Wiley & Sons, Chichester, USA, and Teubner B. G. Stuttgart, Germany.

[6] Peterson V L (1988) Wind Profiling: The History, Principles and Applications of the Clear Air Doppler Radar. Tycho Technology Inc.

[7] Ramm A G, Katsevich A I (1996) The Radon transform and local tomography. CRC Press, Boca Raton, FL.

[8] Rihaczek A W (1971) Radar Waveform Selection - A Simplified Approach. IEEE Trans. Aerospace & Electronics System, Vol. AES-7 pp. 1078–1086.

[9] Sauvageot H (1992) Radar Meteorology. Artech House.

[10] Sharafutdinov V A (1994) Integral Geometry of Tensor Fields. Inverse and Ill-posed Problems Series. VSP, Utrecht.

[11] Sparr G, Stråhlén K, Lindström K, Persson H (1995) Doppler Tomography for Vector Fields. Inverse Problems 11 , no. 5, pp. 1051–1061

[12] Tsang L, Kong J A, Shin R T (1985) Theory of Microwave Remote Sensing. By John Wiley & Sons Inc., Chicester.